STRUCTURAL BIOLOGY

ISSN: 2059-7983
journals.iucr.org/d

1.8 Å resolution crystal structure of the carbapenem intrinsic resistance protein CarF

Evelyn M. Tichy, Steven W. Hardwick, Ben F. Luisi and George P. C. Salmond

Acta Cryst. (2017). D**73**, 549–556

STRUCTURAL BIOLOGY

ISSN 2059-7983

1.8 Å resolution crystal structure of the carbapenem intrinsic resistance protein CarF

Evelyn M. Tichy, Steven W. Hardwick, Ben F. Luisi and George P. C. Salmond*

Department of Biochemistry, University of Cambridge, Building O, Downing Site, Cambridge CB2 1QW, England. *Correspondence e-mail: gpcs2@cam.ac.uk

Received 28 August 2016
Accepted 9 February 2017

Edited by J. L. Martin, Griffith University, Australia

Keywords: antibiotic resistance; carbapenem; intrinsic resistance; CIR family; CLec domain.

PDB reference: CarF, 5aoh

Supporting information: this article has supporting information at journals.iucr.org/d

The natural production of the β-lactam antibiotic carbapenem in bacteria involves a group of enzymes that form a synthetic pathway as well as proteins that protect the cell from self-intoxification by the products. Here, the crystal structure of CarF, one of the two proteins that confer resistance to synthesis of the antibiotic in the host organism, is reported. The CarF fold places it within a widely occurring structural family, indicating an ancient structural origin from which the resistance function has been derived.

1. Introduction

The emergence and increasing prevalence of enterobacterial resistance to carbapenem antibiotics is a growing cause for concern in the medical, public health and scientific communities (McKenna, 2013). As 'antibiotics of last resort', the carbapenems play a key role in the treatment of life-threatening, drug-resistant infections. In particular, the co-occurrence of carbapenem resistance with resistance to other, more commonly used, antibiotics is a worrying trend.

Carbapenem antibiotics are naturally occurring bicyclic β-lactams. The first carbapenem discovered was thienamycin (from *Streptomyces cattleya*) followed by 1-carbapen-2-em-3-carboxylic acid (from *Erwinia*/*Pectobacterium* among others). Although these molecules show antibiotic activity, they are made in low abundance by the producer strains, are readily hydrolysed by renal dihydropeptidases and are too unstable for clinical use (Moellering *et al.*, 1989; Fukasawa *et al.*, 1992). Chemically synthesized derivatives, including imipenem, meropenem and ertapenem, are significantly more stable and are used successfully to combat pathogens expressing extended-spectrum β-lactamases. To date, over 80 carbapenem-derived compounds, most with improved antimicrobial properties and clinical stability, have been described in the literature. However, few of these are currently used clinically (Papp-Wallace *et al.*, 2011). As resistance to the clinically employed carbapenem derivatives continues to evolve under strong selection, and as carbapenem-resistance genes in pathogens are disseminated internationally, understanding of carbapenem-resistance mechanisms is becoming increasingly important.

Production of the simplest carbapenem, 1-carbapen-2-em-3-carboxylic acid, is limited to a small group of enterobacteria, including *Serratia* sp. ATCC 39006 (*S.* 39006), *Photorhabdus luminescens* TT01, *Erwinia herbicola* and various *Erwinia carotovora* subsp. *carotovora* (*Ecc*) strains (now reclassified as *Pectobacterium carotovorum*) (Parker *et al.*, 1982; McGowan *et al.*, 1998; Derzelle *et al.*, 2002; reviewed in Whitehead *et al.*, 2001). However, cryptic *car* gene clusters have been found in a

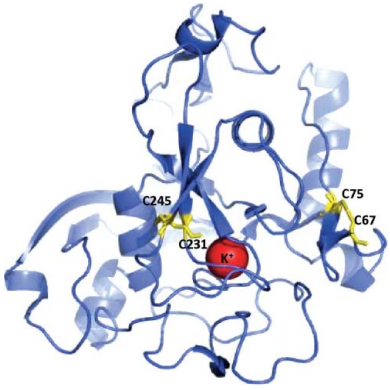

wider range of bacterial strains (Holden *et al.*, 1998). In *Ecc* and *S.* 39006, carbapenem production is controlled by the *car* operon, which includes five well characterized biosynthetic genes (*carA*, *carB*, *carC*, *carD* and *carE*), two carbapenem intrinsic resistance (CIR) genes (*carF* and *carG*) and a gene of unknown function (*carH*). Carbapenem production is controlled by a complex hierarchical regulatory network that includes quorum sensing (Coulthurst *et al.*, 2005).

The control of the *car* cluster in both *Ecc* and *S.* 39006 has been studied extensively. For more information on *car* operon regulation in *Ecc* and *S.* 39006, see Coulthurst *et al.* (2005), Wilf *et al.* (2011), Poulter *et al.* (2011), Clifton *et al.* (2003), Bodner *et al.* (2011), Phelan & Townsend (2013) and Hamed *et al.* (2013). However, the intrinsic resistance mechanism encoded by *carF* and *carG* has been less well studied.

Previous work in *Ecc* has shown that $CarF_{Ecc}$ and $CarG_{Ecc}$ are highly conserved within the group of carbapenem-producing strains. They do not show homology to any proteins known to be involved in antibiotic resistance. CarF and CarG are not able to hydrolyse other β-lactam antibiotics and do not confer cross-resistance to the clinically employed carbapenem imipenem (McGowan *et al.*, 1995, 1996, 1997). Mutagenesis of the resistance genes has shown that CarF and CarG act in concert, each individually conferring partial carbapenem resistance and having complementary and additive effects (McGowan *et al.*, 1997). CarF and CarG have no known sequence similarity and their mechanism(s) of action is, as yet, unknown. Recent studies have shown structural similarities between $CarG_{S.39006}$ and the periplasmic lysozyme inhibitor PliI-Ah (Tichy *et al.*, 2014). The structural similarity between lysozyme and penicillin-binding proteins suggests that $CarG_{S.39006}$-mediated carbapenem resistance may function *via* interaction with the molecular targets of β-lactam antibiotics, the penicillin-binding proteins (PBPs; Tichy *et al.*, 2014).

Formally, there are several possibilities for CarF and CarG to mediate carbapenem resistance. The first possibility would be some alteration of the molecular targets, the PBPs. Secondly, CarF and CarG could modify the cell wall to limit access of the antibiotic to its target. Formally, these carbapenem intrinsic resistance (CIR) proteins might also confer carbapenem resistance by acting as specific β-lactamases (although unlikely), by providing or activating efflux exporters, or *via* the deletion or modification of porin proteins to reduce antibiotic import (Fisher *et al.*, 2005; Drawz & Bonomo, 2010).

Resistance to β-lactam antibiotics in general, and carbapenem antibiotics in particular, has been studied extensively in recent years because of the serious clinical implications of these emerging resistance mechanisms (Nordmann *et al.*, 2011; Nordmann & Poirel, 2013). Various resistance mechanisms in clinically important pathogens have been described, including the production of 'carbapenemases' (Nordmann & Poirel, 2013; Yang *et al.*, 1990; Queenan & Bush, 2007), efflux (Bornet *et al.*, 2003) and the loss and/or modification of porins (Tängdén *et al.*, 2013; Chow & Shlaes, 1991; Armand-Lefèvre *et al.*, 2003; Correa *et al.*, 2013). However, new carbapenem-resistance mechanisms are likely to emerge owing to strong positive selection through widespread use of this class of antibiotics (Nordmann & Poirel, 2013; Walsh *et al.*, 2011).

This study is the first description of the crystal structure of the carbapenem intrinsic resistance protein $CarF_{S.39006}$. The driver for this study was the hypothesis that illuminating the structural characteristics of the CIR-family proteins may help to further our understanding of the existing mechanisms of intrinsic carbapenem resistance. Although the genes encoding the intrinsic resistance mechanism have not yet appeared in clinical drug-resistant isolates, advances in our basic knowledge about CIR-family proteins may help to predict future mechanisms of emerging clinical resistance to this increasingly endangered class of antibiotics.

Table 1
Macromolecule-production information.

Cleavage sites are shown in italics for oligonucleotides and the added hexahistidine tag is underlined.

Source organism	*Serratia* sp. ATCC 39006
DNA source	*Serratia* sp. ATCC 39006
Forward primer	GAT*GAATTC*ATTAAAGAGGAGAAATTAACTATGT-ATTAAAGAGGAGAAATTAACTATGTTGAAAAA-TCGTATT
Reverse primer	GTC*AAGCTT*AGTGATGGTGATGGTGATGTTTATC-GTGATGGTGATGGTGATGTTTATCATCGATCG-GCCT
Cloning vector	pQE80*oriT*
Expression vector	pQE80*oriT*
Expression host	*Serratia* sp. ATCC 39006
Complete amino-acid sequence of the construct produced	EILPIDEVNVDGGDFYVGLVFGKEDYAAHANTHL-TPFSIMRTEVTYHQYQALQAWAETRGYQISGG-CNGATFEDCWPSEKDGGRHPVTNVSWWDAVIF-ANALSAQHNLQPYYVTADGQALKIPPEEGTDR-GIRENPQASGYRLPTLAEWQVAARGGNKGLSD-GTYGSRYAGKDQPASVANLPVSGTQTFSTLPV-ASKQPNSLGLYDMSGNVSEWLNENYAVKGGKK-MYYFCGGSYMDRVGSLASCDVHTPGFAMSDIG-FRLVRPIDDK<u>HHHHHH</u>

2. Experimental procedures

2.1. Overexpression and purification

Recombinant $CarF_{S.39006}$ with a C-terminal hexahistidine tag was expressed in *S.* 39006 under the control of the IPTG-inducible T7 promoter in plasmid pQE80*oriT*. The plasmids and primers used for cloning are summarized in Table 1. The protein was purified and crystallized according to the protocol previously published for $CarG_{S.39006}$ (Tichy *et al.*, 2014), but with some modifications. In brief, $CarF_{S.39006}$ was purified from clarified whole-cell lysate with Ni–NTA agarose (Qiagen) according to the manufacturer's guidelines [lysis buffer: 50 m*M* NaH_2PO_4, 300 m*M* NaCl, 10 m*M* imidazole, 0.01% Triton X-100 (pH 7.5)]. Elution fractions were pooled and dialysed overnight against low-salt buffer (20 m*M* NaCl, 50 m*M* Tris–HCl pH 7.5, 1 m*M* DTT, 0.01% Triton X-100) prior to further purification using a HiTrap Q Sepharose anion-exchange column (GE Life Sciences). Further purification was performed by gel-filtration chromatography of pooled, concentrated elution fractions using a Superdex 75 column (GE Life Sciences) in 100 m*M* NaCl, 50 m*M* Tris, 1 m*M* DTT, 0.05% Triton X-100 (pH 7.5). Detergent was

Table 2
Crystallization.

Method	Vapour diffusion, sitting drop
Plate type	MRC 2-drop, 96-well
Temperature (K)	291
Protein concentration (mg ml^{-1})	10
Buffer composition of protein solution	100 m*M* NaCl, 50 m*M* Tris, 1 m*M* DTT pH 7.5
Composition of reservoir solution	0.1 *M* Morpheus Carboxylic Acids, 0.1 *M* HEPES/MOPS pH 7.5, 17.5% MPD, 17.5% PEG 1000, 17.5% PEG 3350
Volume and ratio of drop	0.4 µl, 1:1
Volume of reservoir (µl)	70

Table 3
Data collection and processing.

Values in parentheses are for the outer shell.

Diffraction source	Beamline I04, DLS
Wavelength (Å)	0.978
Temperature (K)	180
Detector	PILATUS pixel
Crystal-to-detector distance (mm)	190.5
Rotation range per image (°)	0.2
Total rotation range (°)	90.0
Exposure time per image (s)	0.2
Space group	$P2_12_12_1$
a, *b*, *c* (Å)	49.47, 55.45, 176.20
α, β, γ (°)	90, 90, 90
Mosaicity (°)	0.16
Resolution range (Å)	36.13–1.80
Total No. of reflections	144044 (9084)
No. of unique reflections	44709 (2788)
Completeness (%)	97.5 (99.1)
Multiplicity	3.2 (3.3)
$\langle I/\sigma(I)\rangle$	8.0 (2.0)
$R_{\rm r.i.m.}$	0.12 (0.56)
Overall *B* factor from Wilson plot (Å^2)	16.077

removed from the final concentrated sample by dialysis with BioBeads SM-2 Adsorbent Beads (Bio-Rad) according to the manufacturer's instructions. The hexahistidine tag did not affect protein function, as demonstrated by the *E. coli* ESS carbapenem lethality bioassay described previously (McGowan *et al.*, 1997; see Supporting Information).

2.2. Crystallization, X-ray data collection, structure determination and refinement

The initial crystallization condition for CarF was identified using a commercial screen (Morpheus, Molecular Dimensions) by the sitting-drop vapour-diffusion method at 18°C. The final optimized crystals were obtained in a precipitant solution consisting of 0.1 *M* Morpheus Carboxylic Acids, 0.1 *M* HEPES/MOPS pH 7.5, 17.5% MPD, 17.5% PEG 1000, 17.5% PEG 3350, again using the sitting-drop vapour-diffusion method (Table 2). The crystals were flash-cooled in liquid nitrogen using crystallization mother liquor supplemented with 25% glycerol as a cryoprotectant. X-ray diffraction data were collected from a single crystal of CarF on beamline I04 at Diamond Light Source (DLS) to 1.8 Å resolution and were processed using *iMosflm* (Battye *et al.*, 2011) and *AIMLESS* (Evans & Murshudov, 2013) in the *CCP*4 program suite (Winn *et al.*, 2011). Initial phase estimates and

Table 4
Structure solution and refinement.

Values in parentheses are for the outer shell.

Resolution range (Å)	36.13–1.80
Completeness (%)	97.2
σ Cutoff	2.44
No. of reflections, working set	44709
No. of reflections, test set	2185
Final $R_{\rm cryst}$	0.137
Final $R_{\rm free}$	0.208
Cruickshank DPI	0.267
No. of non-H atoms	
Protein	3983
Ion	2
Water	305
Total	4290
R.m.s. deviations	
Bonds (Å)	0.019
Angles (°)	1.87
Average *B* factors (Å^2)	
Protein	24.99
Ion	21.23
Water	37.95
Ramachandran plot	
Most favoured (%)	96.15
Allowed (%)	3.46

electron-density maps were calculated by molecular replacement with *Phaser* (McCoy *et al.*, 2007) using an ensemble of CarF models generated by the *Robetta de novo* protein-modelling webserver (Raman *et al.*, 2009) as initial search models (Kim *et al.*, 2004). Structural refinement of the initial model was performed using restrained refinement in *REFMAC*5 with jelly-body refinement and anisotropic temperature factors (Murshudov *et al.*, 2011), in combination with iterative model building with *Coot* (Emsley & Cowtan, 2004). Noncrystallographic symmetry restraints were not used during structure refinement. The quality of the final model was assessed with *MolProbity* (Chen *et al.*, 2010) and the geometry and all-atom contacts were ranked in the 92nd percentile in comparison to structures of similar resolution (data-collection and refinement statistics are summarized in Tables 3 and 4).

2.3. Carbapenem-resistance bioassay

Carbapenem resistance in the bacterial strains of interest was assayed using the *E. coli* ESS killing bioassay described previously (McGowan *et al.*, 1997). In essence, the *E. coli* strain ESS is supersensitive to β-lactam antibiotics and therefore enables the detection of low concentrations of the carbapenem antibiotic made by the producer strain. In contrast, recombinant *E. coli* ESS expressing cloned *carF* and *carG* genes (for intrinsic resistance to the carbapenem) exhibit significantly decreased sensitivity to the antibiotic, as shown previously (McGowan *et al.*, 1997).

2.4. Analytical gel filtration

CarF$_{S.39006}$ complex formation was assayed by analytical gel filtration as described by Whitaker (1963), using hexahistidine-tagged CarF$_{S.39006}$ purified as described above. Gel filtration was performed on an S-200 analytical gel-filtration column (GE Healthcare) and the elution volumes were compared with

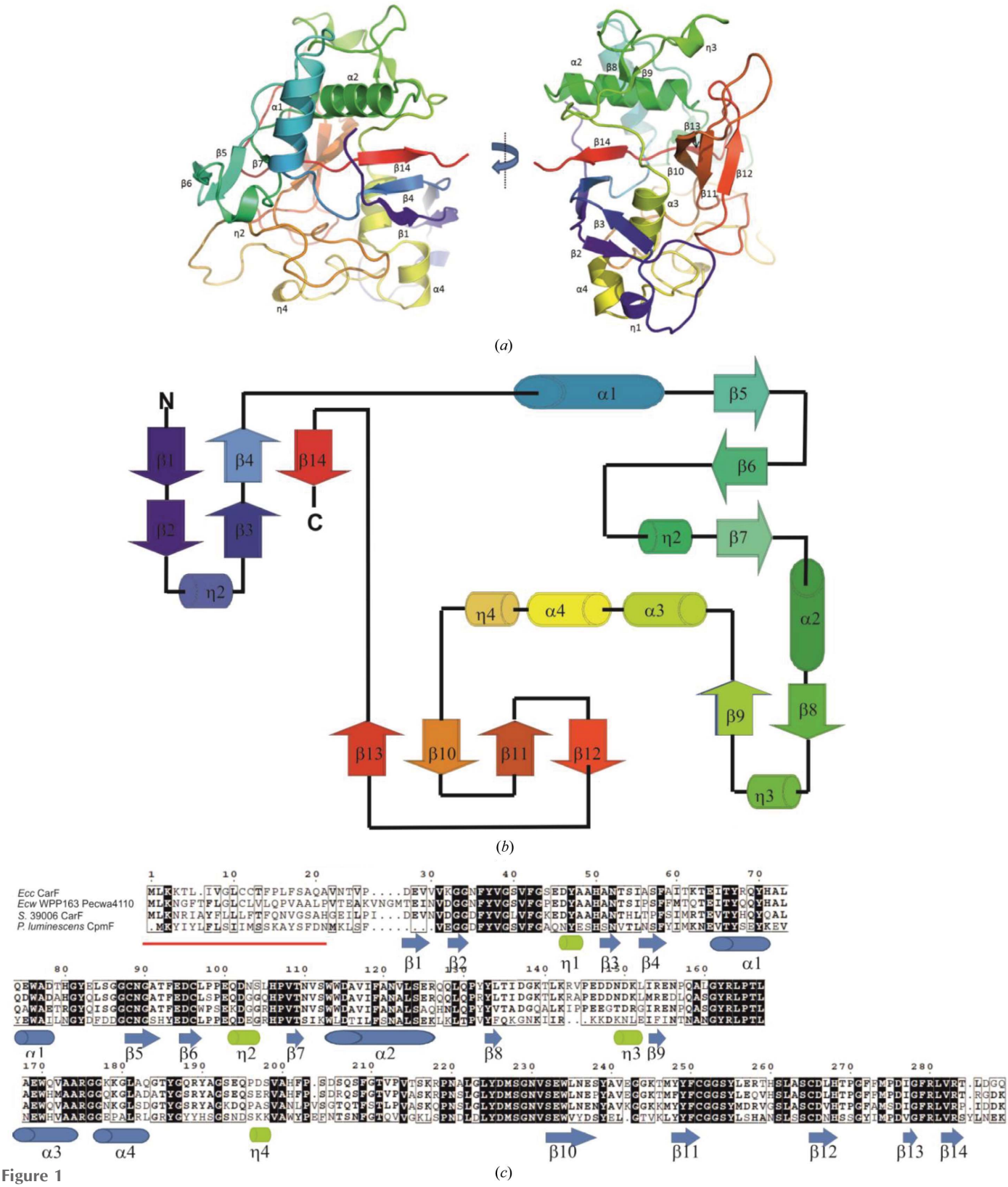

Figure 1

The structure of $CarF_{S.39006}$. (*a*) Two orthogonal views of CarF depicted as a cartoon representation. The CarF monomer is coloured as a rainbow (blue to red from the N- to C-terminus) and secondary-structural elements are labelled. (*b*) Topology diagram of $CarF_{S.39006}$, with structural features coloured to correspond to (*a*). (*c*) Structure-based sequence alignment of CarF and its known functional homologues. CarF secondary-structure elements are indicated below the protein sequences. Amino acids are shaded in accordance with CarF sequence conservation. A black background indicates a fully conserved residue. The observed secondary-structural elements in the crystal structure of CarF are numbered sequentially. α-Helices are shown as blue cylinders, 3_{10}-helices as green cylinders and β-strands as blue arrows. Atomic coordinates and structure-factor files have been deposited with the PDB (PDB entry 5aoh).

those obtained using standards of known molecular mass (Gel Filtration Markers Kit for Protein Molecular Weights 12 000–200 000 Da; Sigma–Aldrich).

3. Results

The crystallographic asymmetric unit contains two protomers of CarF related by a twofold noncrystallographic symmetry axis. Analysis of the oligomeric state using *PISA* (Krissinel & Henrick, 2007) indicates that the buried surface area formed by the dimer seen in the asymmetric unit is 2090 Å^2 (9.9% of the total surface area of the dimer). Although this interface is sufficiently extensive for the dimer to be stable in solution (Krissinel & Henrick, 2007), we propose that it is a non-biological artefact of the crystal lattice. Analytical gel filtration of CarF$_{S.39006}$ shows that the protein elutes at a volume corresponding to a molecular mass of 25 kDa, which is consistent with the predicted monomer of hexahistidine-tagged CarF, which has a molecular mass of 30.0 kDa (see Supporting Information).

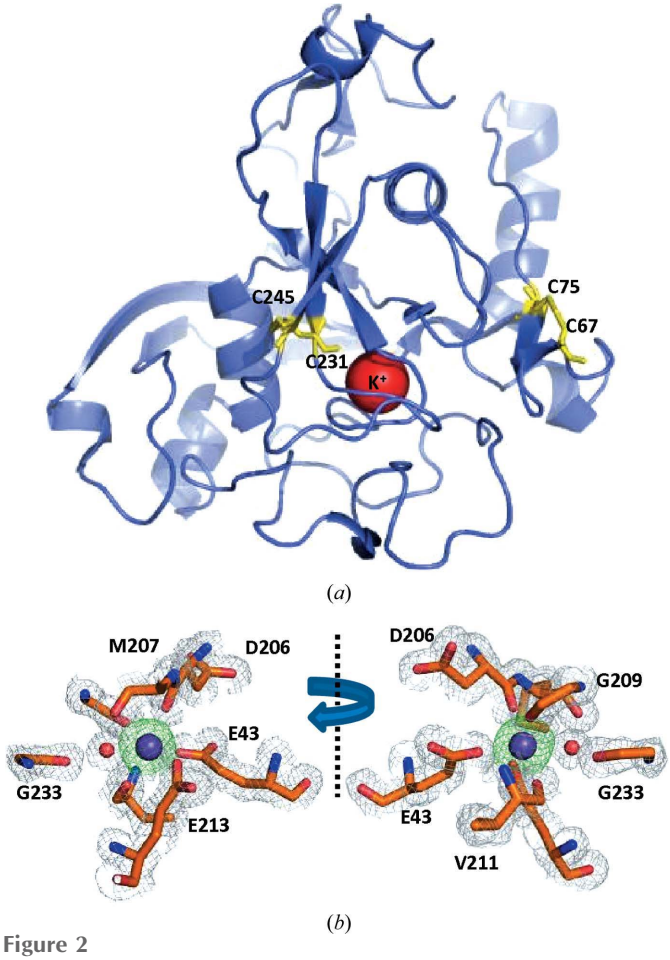

Figure 2
Structural features of CarF. (*a*) Disulfide bonds. A monomer of CarF is shown as a blue cartoon. Residues involved in intramolecular disulfide bonds are shown as yellow sticks and are labelled. The putative potassium ion is shown as a red sphere. (*b*) Putative metal ion. Two orthogonal views of a putative potassium ion bound in the CarF structure. The potassium ion is shown as a purple sphere, a coordinated water molecule is shown as a red sphere and amino-acid residues involved in metal-ion coordination are shown as sticks. The $2F_o - F_c$ electron-density map for this region is shown as a grey mesh contoured at 1σ, and the $F_o - F_c$ map calculated with the potassium ion omitted is shown as a green mesh contoured at 3σ.

The structure of CarF$_{S.39006}$ and its secondary-structural elements are depicted in Fig. 1. In general, CarF$_{S.39006}$ has low secondary-structure content (20% α-helix and 19% β-strand). The N-terminus is composed of several short β-strands (β1–β4). These form two separate antiparallel sheets which wrap around the surface of the C-terminal helices α3 and α4. On the opposite surface of the CarF$_{S.39006}$ monomer, helices α1 and α2 pack such that they cross at nearly right angles. The only other secondary-structural elements are four short β-strands which form a short four-stranded antiparallel sheet in the centre of the molecule (strands β10–β13). Sequence conservation of CarF and known functional homologues are shown in Fig. 1(*c*). Mapping the conserved residues to the surface of CarF reveals that amongst the general distribution of the position of the conserved residues, a clustered belt of conserved residues is present on one face of CarF, encompassing sheets formed of strands β1–β2 and β10–β12 and a large region of low secondary structure (Supplementary Fig. S3).

The electron-density maps revealed the presence of a potential bound metal ion. The putative metal ion has octahedral coordination and involves the side chains of Glu43 and Glu213, carbonyl O atoms from Asp206, Gly209 and Val211, and a nearby water molecule (see Fig. 2*b*). Given the octahedral coordination of the metal ion this was likely to be either sodium, potassium or calcium. When modelling this potential ion as water and running the 'highly coordinated waters' option in *Coot*, this atom was suggested to be either potassium or calcium. Elemental ion placement in *phenix.refine* suggested this ion to be calcium. However, given that both sodium and potassium salts were present in the crystallization solution as part of the Morpheus Carboxylic Acids mix, potassium was modelled into the observed electron density following refinement. The putative potassium is buried within the CarF$_{S.39006}$ monomer and may function to stabilize the loops within this region of low secondary structure. Both CarF$_{S.39006}$ protomers contain two intramolecular disulfide bonds (Cys67–Cys75 and Cys231–Cys245). Both of these disulfide links appear to stabilize sheet structures, with the paired residues 67 and 75 bridging strands 5 and 6, and residues 231 and 245 bridging strands 11 and 12 (see Fig. 2*a*).

Structural homologues of CarF$_{S.39006}$ were identified *via* the *DALI* protein structural database server (Holm & Rosenström, 2010). The top-scoring structural matches for CarF$_{S.39006}$ consisted primarily of proteins with an FGE domain (formyl-glycine generating enzymes). CarF$_{S.39006}$ superimposes onto the human FGE protein with a core r.m.s.d. of 1.43 Å over 176 aligned residues (30% amino-acid sequence identity; PDB entry 1y1j; Dierks *et al.*, 2005) and confirms that CarF does indeed consist of an FGE-like domain beginning at Pro36 and continuing to the C-terminus of CarF$_{S.39006}$ (Fig. 3*a*). Using the amino-acid sequence of CarF$_{S.39006}$ as a query for an iterative hidden Markov motif search with the *Jackhmmer* web server (Murzin *et al.*, 1995), the Pfam domain FGE-sulfatase (PF03781.14) was identified spanning residues

27–286 of the input sequence. Further analysis with *Jackhmmer* reveals 2439 sequences in the Pfam database containing the FGE-sulfatase domain, often as part of a multidomain protein. The FGE domain is a subtype of the C-type lectin (CLec) fold (Finn *et al.*, 2015) and it has been proposed that like the Ig fold and the leucine-rich repeat fold, the CLec fold can be considered as a stable structural template to allow massive sequence variation in enzymes of varying function (Coq & Ghosh, 2011). The ability of such proteins to accommodate such massive sequence variability has been proposed as a mechanism for these proteins to bind to novel ligands, and may in part explain the diversity of proteins that this domain is found in. In the $CarF_{S.39006}$ structure the N- and C-termini of the CLec domain form β-strands that pair with one another (strands β4 and β14). In $CarF_{S.39006}$ there is an N-terminal extension to the C-Lec domain. This extension wraps around the surface of the CLec domain and may serve to mask hydrophobic residues in this region. Residues 108–141 of $CarF_{S.39006}$ correspond to a region which is variable within FGE proteins. In TvpA of *Treponema denticola* this variable region appears to stabilize helix α1, and this region may play a similar role in $CarF_{S.39006}$ (Coq & Ghosh, 2011).

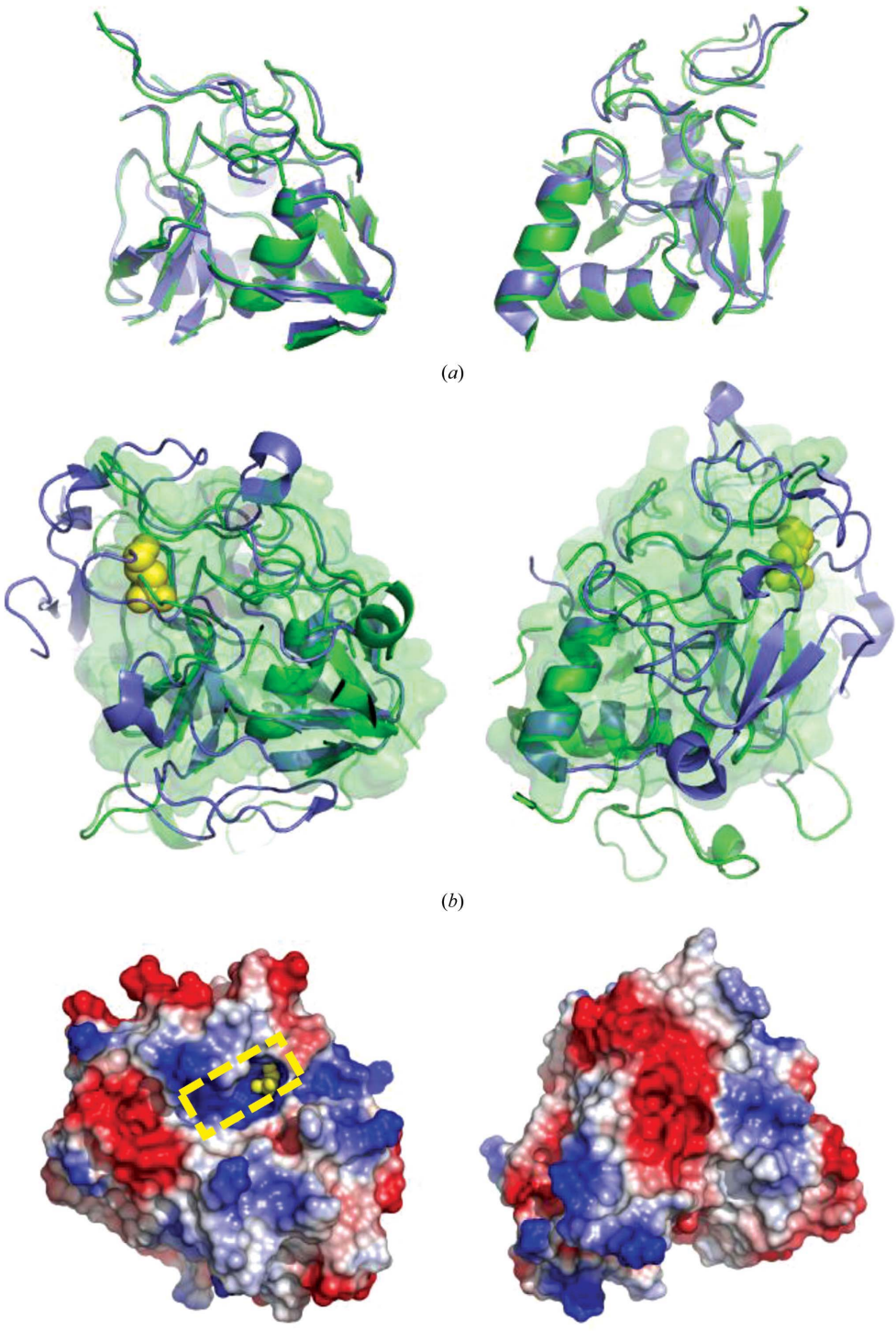

Figure 3
The FGE active site is not conserved in $CarF_{S.39006}$. (*a*) Two orthogonal views of the structurally conserved regions of CarF (green) overlaid on human FGE (blue). (*b*) Two orthogonal views of the entire CarF structure (green) overlaid on human FGE (blue, with the active-site cysteines as yellow spheres). The orientation of the views are as in (*a*) and the boundary of the structurally conserved core is shown as a semi-transparent surface. (*c*) Electrostatic surfaces of hFGE (left) and CarF (right) in the same orientation. The FGE active-site channel highlighted by the yellow dashed box (with the active-site cysteine in yellow) is not present in CarF.

FGE-type enzymes act by oxidizing cysteine or serine to produce formylglycine, which is a critical active-site residue of sulfatases. The active site of FGE proteins bears a groove containing proline and reactive cysteine residues, which are critical for catalysis (Dierks *et al.*, 2005). A comparison of $CarF_{S.39006}$ with the catalytically active human FGE protein is shown in Fig. 3(*b*), with the active-site cysteine highlighted. The overlay shows that although the general FGE-domain structure is conserved in $CarF_{S.39006}$, the region around the active site is not. The substrate-binding groove present in human FGE

appears as a flat surface in the $CarF_{S.39006}$ structure and, more importantly, the reactive cysteine is absent. Taken together, these data would suggest that CarF does not function as a bona fide formyl-glycine generating enzyme, despite the structural similarities.

4. Discussion

In this study, we describe the X-ray crystallographic structure of $CarF_{S.39006}$, a member of the CIR family of proteins. Earlier structural analyses of the co-operonic $CarG_{S.39006}$ showed structural similarities to prokaryotic lysozyme inhibitors (Tichy *et al.*, 2014). Here, we find that $CarF_{S.39006}$ also shows structural homology to known proteins but has not retained the relevant catalytic residues. The precise mechanism of action of $CarF_{S.39006}$ in carbapenem resistance has yet to be elucidated, but is likely to include regulatory interaction with a partner protein or other macromolecule.

In light of the known homologies, it has been postulated that $CarG_{S.39006}$ may act by interaction with the molecular targets of carbapenem antibiotics, namely the penicillin-binding proteins (Tichy *et al.*, 2014). Recent, preliminary research conducted in this laboratory has suggested that $CarF_{S.39006}$ may interact with outer membrane porins in Gram-negative bacteria. Consequently, it is tempting to speculate that the additive resistance-conferring functions of $CarF_{S.39006}$ and $CarG_{S.39006}$ in conferring resistance to carbapenem may be owing to distinct, yet complementary, mechanisms. This could be mediated by the protection, modification or sequestration of the target molecule by CarG coupled with the inhibition or diminution of antibiotic uptake through porin modification by CarF. While it has not yet been possible to determine the exact molecular mechanism by which CarF and CarG confer resistance to the carbapenem, the structural data identified a number of interesting sites for further mutagenesis studies.

In the face of the continuing emergence of clinically relevant carbapenem-resistant strains, understanding how naturally occurring carbapenem-resistance mechanisms have evolved may be increasingly relevant, particularly as clinically relevant drug resistance is known to be at least partially driven by horizontal gene transfer from nonpathogenic strains (Nordmann & Poirel, 2013; Walsh *et al.*, 2011). The structural determination of the two essential carbapenem-resistance proteins will contribute to a broader understanding of enterobacterial carbapenem resistance.

Acknowledgements

The authors would like to thank Jarrod Voss for his advice on protein purification and crystallography, Harry Jubb for bioinformatic analyses and Dima Chirgadze for help with crystallization equipment and X-ray diffraction data collection. X-ray diffraction data were collected on beamline I04-1 at Diamond Light Source. This work was supported by a Herchel Smith PhD scholarship to EMT. BFL is supported by the Wellcome Trust and work in the Salmond laboratory is supported by the Biotechnology and Biological Sciences Research Council, UK.

References

Armand-Lefèvre, L., Leflon-Guibout, V., Bredin, J., Barguellil, F., Amor, A., Pagès, J. M. & Nicolas-Chanoine, M.-H. (2003). *Antimicrob. Agents Chemother.* **47**, 1165–1168.
Battye, T. G. G., Kontogiannis, L., Johnson, O., Powell, H. R. & Leslie, A. G. W. (2011). *Acta Cryst.* D**67**, 271–281.
Bodner, M. J., Li, R. F., Phelan, R. M., Freeman, M. F., Moshos, K. A., Lloyd, E. P. & Townsend, C. A. (2011). *Chembiochem*, **12**, 2159–2165.
Bornet, C., Chollet, R., Malléa, M., Chevalier, J., Davin-Regli, A., Pagès, J.-M. & Bollet, C. (2003). *Biochem. Biophys. Res. Commun.* **301**, 985–990.
Chen, V. B., Arendall, W. B., Headd, J. J., Keedy, D. A., Immormino, R. M., Kapral, G. J., Murray, L. W., Richardson, J. S. & Richardson, D. C. (2010). *Acta Cryst.* D**66**, 12–21.
Chow, J. & Shlaes, D. M. (1991). *J. Antimicrob. Chemother.* **28**, 499–504.
Clifton, I. J., Doan, L. X., Sleeman, M. C., Topf, M., Suzuki, H., Wilmouth, R. C. & Schofield, C. J. (2003). *J. Biol. Chem.* **278**, 20843–20850.
Correa, L., Martino, M., Siqueira, I., Pasternak, J., Gales, A. C., Silva, C. V., Camargo, T. Z. S., Scherer, P. F. & Marra, A. R. (2013). *BMC Infect. Dis.* **13**, 80.
Coulthurst, S. J., Barnard, A. M. L. & Salmond, G. P. C. (2005). *Nature Rev. Microbiol.* **3**, 295–306.
Derzelle, S., Duchaud, E., Kunst, F., Danchin, A. & Bertin, P. (2002). *Appl. Environ. Microbiol.* **68**, 3780–3789.
Dierks, T., Dickmanns, A., Preusser-Kunze, A., Schmidt, B., Mariappan, M., von Figura, K., Ficner, R. & Rudolph, M. G. (2005). *Cell*, **121**, 541–552.
Drawz, S. M. & Bonomo, R. A. (2010). *Clin. Microbiol. Rev.* **23**, 160–201.
Emsley, P. & Cowtan, K. (2004). *Acta Cryst.* D**60**, 2126–2132.
Evans, P. R. & Murshudov, G. N. (2013). *Acta Cryst.* D**69**, 1204–1214.
Finn, R. D., Clements, J., Arndt, W., Miller, B. L., Wheeler, T. J., Schreiber, F., Bateman, A. & Eddy, S. R. (2015). *Nucleic Acids Res.* **43**, W30–W38.
Fisher, J. F., Meroueh, S. O. & Mobashery, S. (2005). *Chem. Rev.* **105**, 395–424.
Fukasawa, M., Sumita, Y., Harabe, E. T., Tanio, T., Nouda, H., Kohzuki, T., Okuda, T., Matsumura, H. & Sunagawa, M. (1992). *Antimicrob. Agents Chemother.* **36**, 1577–1579.
Hamed, R. B., Gomez-Castellanos, J. R., Henry, L., Ducho, C., McDonough, M. A. & Schofield, C. J. (2013). *Nat. Prod. Rep.* **30**, 21–107.
Holden, M. T. G., McGowan, S. J., Bycroft, B. W., Stewart, G. S. A. B., Williams, P. & Salmond, G. P. C. (1998). *Microbiology*, **144**, 1495–1508.
Holm, L. & Rosenström, P. (2010). *Nucleic Acids Res.* **38**, W545–W549.
Kim, D., Chivian, D. & Baker, D. (2004). *Nucleic Acids Res.* **32**, W526–W531.
Krissinel, E. & Henrick, K. (2007). *J. Mol. Biol.* **372**, 774–797.
Le Coq, J. & Ghosh, P. (2011). *Proc. Natl Acad. Sci. USA*, **108**, 14649–14653.
McCoy, A. J., Grosse-Kunstleve, R. W., Adams, P. D., Winn, M. D., Storoni, L. C. & Read, R. J. (2007). *J. Appl. Cryst.* **40**, 658–674.
McGowan, S., Sebaihia, M., Jones, S., Yu, B., Bainton, N., Chan, P. F., Bycroft, B., Stewart, G. S. A. B., Williams, P. & Salmond, G. P. C. (1995). *Microbiology*, **141**, 541–550.
McGowan, S. J., Sebaihia, M., O'Leary, S., Hardie, K. R., Williams, P., Stewart, G. S. A. B., Bycroft, B. W. & Salmond, G. P. C. (1997). *Mol. Microbiol.* **26**, 545–556.

McGowan, S. J., Sebaihia, M., Porter, L. E., Stewart, G. S. A. B., Williams, P., Bycroft, B. W. & Salmond, G. P. C. (1996). *Mol. Microbiol.* **22**, 415–426.
McGowan, S. J., Bycroft, B. W. & Salmond, G. P. C. (1998). *Trends Microbiol.* **6**, 203–208.
McKenna, M. (2013). *Nature (London)*, **499**, 394–396.
Moellering, R. C. Jr, Eliopoulos, G. M. & Sentochnik, D. E. (1989). *J. Antimicrob. Chemother.* **24**, Suppl. A, 1–7.
Murshudov, G. N., Skubák, P., Lebedev, A. A., Pannu, N. S., Steiner, R. A., Nicholls, R. A., Winn, M. D., Long, F. & Vagin, A. A. (2011). *Acta Cryst.* D**67**, 355–367.
Murzin, A. G., Brenner, S. E., Hubbard, T. & Chothia, C. (1995). *J. Mol. Biol.* **247**, 536–540.
Nordmann, P., Naas, T. & Poirel, L. (2011). *Emerg. Infect. Dis.* **17**, 1791–1798.
Nordmann, P. & Poirel, L. (2013). *J. Antimicrob. Chemother.* **68**, 487–489.
Papp-Wallace, K. M., Endimiani, A., Taracila, M. A. & Bonomo, R. A. (2011). *Antimicrob. Agents Chemother.* **55**, 4943–4960.
Parker, W., Rathnum, M., Wells, J. S. Jr, Trejo, W. H., Principe, P. A. & Sykes, R. B. (1982). *J. Antibiot.* **35**, 653–660.
Phelan, R. & Townsend, C. (2013). *J. Am. Chem. Soc.* **135**, 7496–7502.
Poulter, S., Carlton, T. M., Spring, D. R. & Salmond, G. P. C. (2011). *Mol. Microbiol.* **80**, 1120–1131.
Queenan, A. M. & Bush, K. (2007). *Clin. Microbiol. Rev.* **20**, 440–458.
Raman, S. *et al.* (2009). *Proteins*, **77**, Suppl. 9, 89–99.
Tängdén, T., Adler, M., Cars, O., Sandegren, L. & Löwdin, E. (2013). *J. Antimicrob. Chemother.* **68**, 1319–1326.
Tichy, E., Luisi, B. & Salmond, G. (2014). *J. Mol. Biol.* **426**, 1958–1970.
Walsh, T. R., Weeks, J., Livermore, D. M. & Toleman, M. A. (2011). *Lancet Infect. Dis.* **11**, 355–362.
Whitaker, J. R. (1963). *Anal. Chem.* **35**, 1950–1953.
Whitehead, N. A., Barnard, A. M. L., Slater, H., Simpson, N. J. L. & Salmond, G. P. C. (2001). *FEMS Microbiol. Rev.* **25**, 365–404.
Wilf, N. M., Williamson, N. R., Ramsay, J. P., Poulter, S., Bandyra, K. J. & Salmond, G. P. C. (2011). *Environ. Microbiol.* **13**, 2649–2666.
Winn, M. D. *et al.* (2011). *Acta Cryst.* D**67**, 235–242.
Yang, Y. J., Wu, P. J. & Livermore, D. M. (1990). *Antimicrob. Agents Chemother.* **34**, 755–758.